Electronic Supplementary Material (ESI) for Analyst.

SUPPLEMENTAL MATERIAL

A Novel Multivariate Curve Resolution-Alternating Least Squares (MCR-ALS) Methodology for Application in Hyperspectral Raman Imaging Analysis

Joseph P. Smith*[1], Erin C. Holahan[2], Frank C. Smith[3], Veronica Marrero[2], and Karl S. Booksh*[2]

[1]Analytical Research & Development, Merck Research Laboratories, Merck & Co., Inc., Rahway, NJ 07065

[2]Department of Chemistry & Biochemistry, University of Delaware, Newark DE 19716

[3]Department of Geological Sciences, University of Delaware, Newark DE 19716

[*]Corresponding Authors:

Joseph P. Smith. Tel: (732) 594-0194. Email: joseph.smith@merck.com

Karl S. Booksh. Tel: (302) 831-2561. Email: kbooksh@udel.edu

RESULTS AND DISCUSSION

S1. OPTICAL MICROSCOPY AND SCANNING ELECTRON MICROSCOPY (SEM). Optical and backscattered electron (BSE) images of grains z3-13 (**Figure S1**) and z4-1 (**Figure S2**) display that both grains are heterogeneous and comprised of polydispersed micrometer- and sub-micrometer-sized particles of varying shape. The displayed physical properties of these grains can be compared with the distribution of the chemical species within them as determined from MCR-ALS applied to hyperspectral Raman imaging.

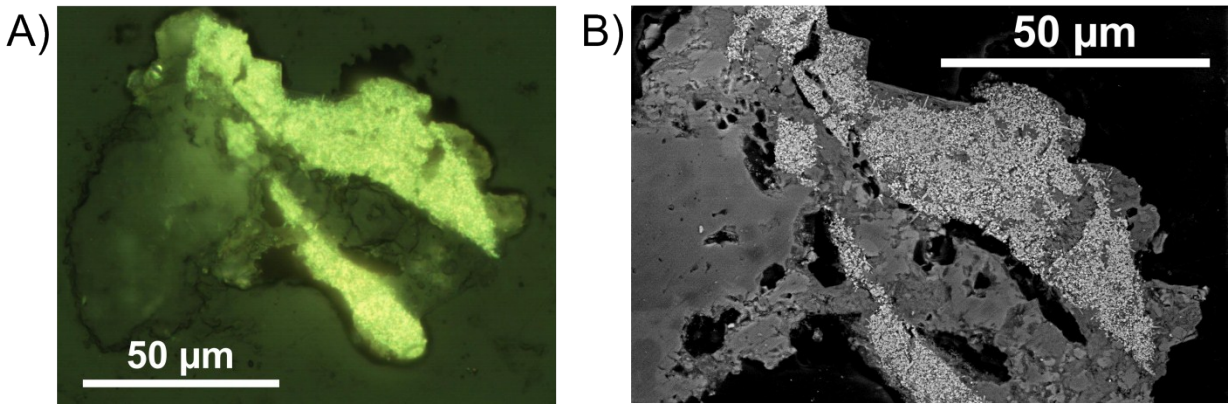

Figure S1: Optical image (A) and backscattered electron (BSE) image (B) of grain z3-13 recovered from the Monteville spherule layer (MSL). Hyperspectral Raman imaging data set Ra15 (Table 1) was collected on this grain.

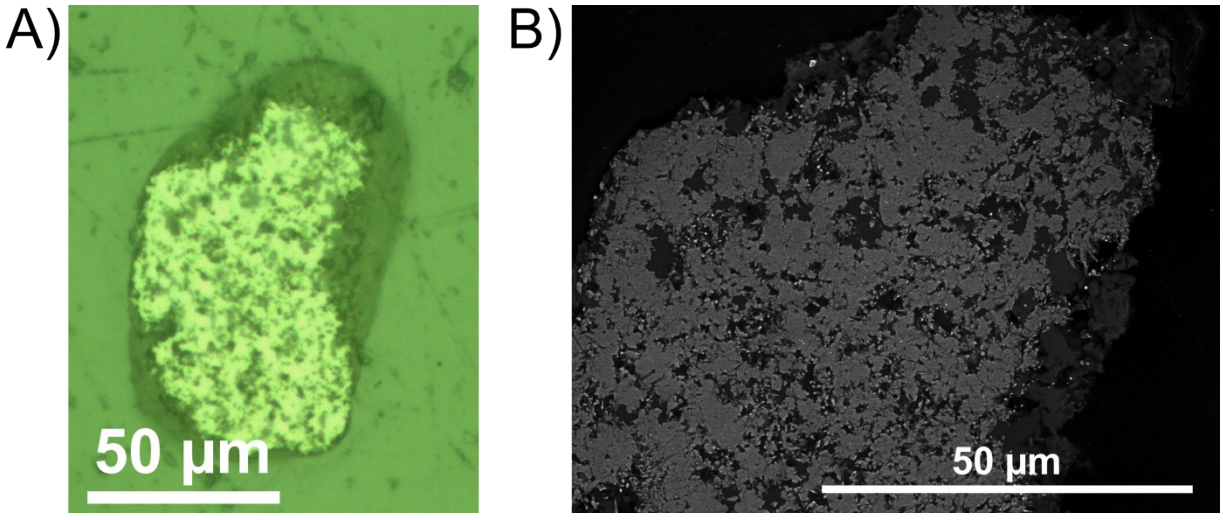

Figure S2: Optical image (A) and backscattered electron (BSE) image (B) of grain z4-1 recovered from the Bee Gorge spherule layer (BGSL). Hyperspectral Raman imaging data set Ra23 (Table 1) was collected on this grain.

S2. MULTIVARIATE CURVE RESOLUTION-ALTERNATING LEAST SQUARES (MCR-ALS) APPLIED TO 27 HYPERSPECTRAL RAMAN IMAGING DATA SETS: CORRELATION OF RESOLVED RAMAN SPECTRA GENERATED FROM MCR-ALS WITH TARGET RAMAN SPECTRA OF REFERENCE MATERIALS. Multivariate curve resolution-alternating least squares (MCR-ALS) was applied to 27 hyperspectral Raman imaging data sets (**Table 1**), most of which are directly available in Smith et al.[1] The resolved Raman spectra generated from MCR-ALS are quantitatively compared to target Raman spectra of reference materials, and the correlation results are reported as correlation coefficients (R^2). Correlation results for hyperspectral Raman imaging data sets Ra15 and Ra23 are displayed in **Figures 1–2** and **Figures 4 and 7**, respectively. Full MCR-ALS results, including spatially resolved chemical images with corresponding resolved Raman spectra, for hyperspectral Raman imaging data sets Ra15 and Ra23 are shown in **Figures S3 and S4**, respectively. The optimal MCR-ALS models were built using 10 components for Ra15 (**Figure S3**) and 11 components for Ra23 (**Figure S4**). Correlation results for the remaining 25 hyperspectral Raman imaging data sets are displayed in **Figures S5-S29**.

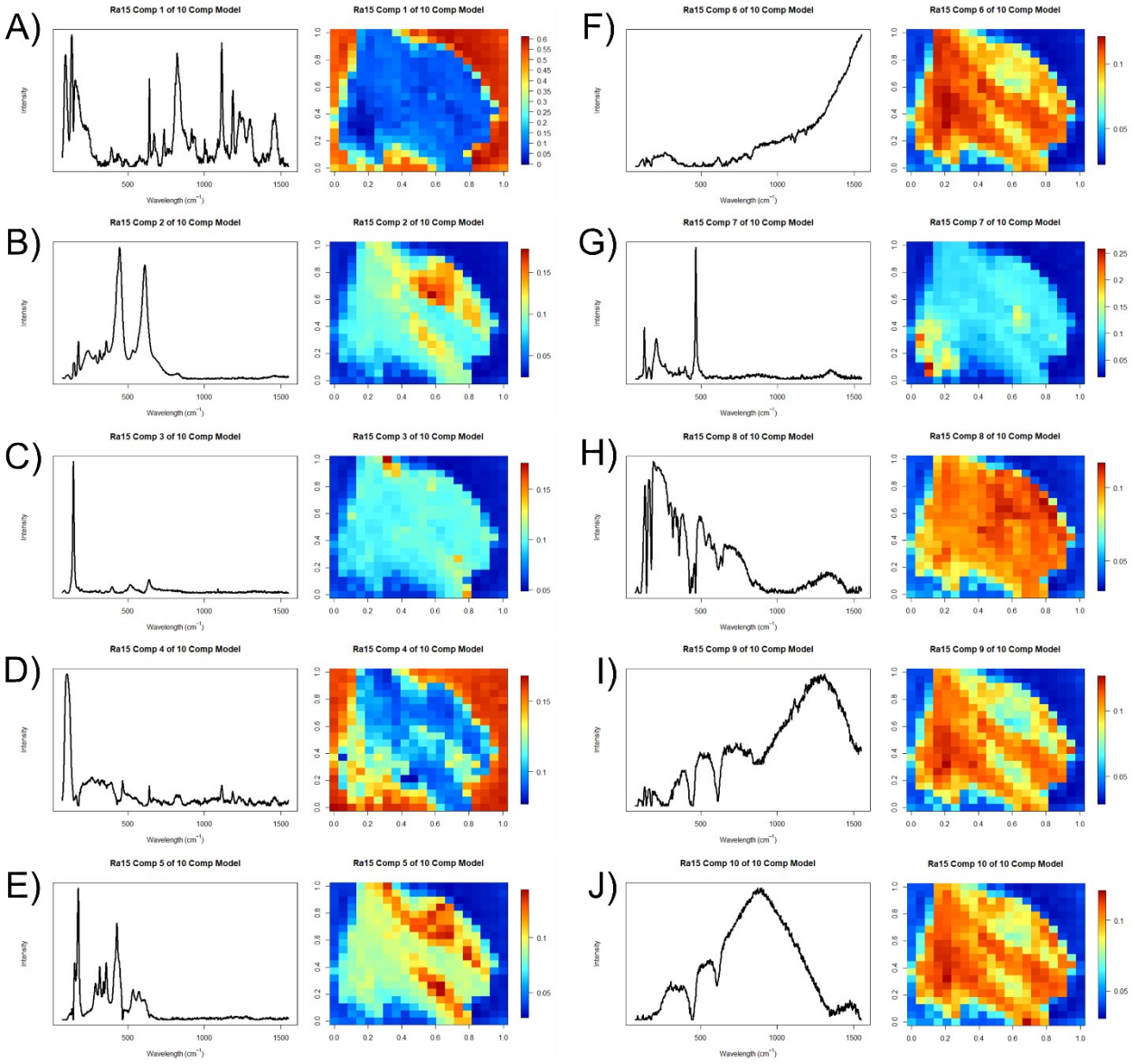

Figure S3: Full MCR-ALS results for hyperspectral Raman imaging data set Ra15. Spatially-resolved chemical images and corresponding resolved Raman spectra generated from a 10 component MCR-ALS model applied to hyperspectral Raman imaging data set Ra15 are shown for each component—component 1 (A), component 2 (B), component 3 (C), component 4 (D), component 5 (E), component 6 (F), component 7 (G), component 8 (H), component 9 (I), and component 10 (J).

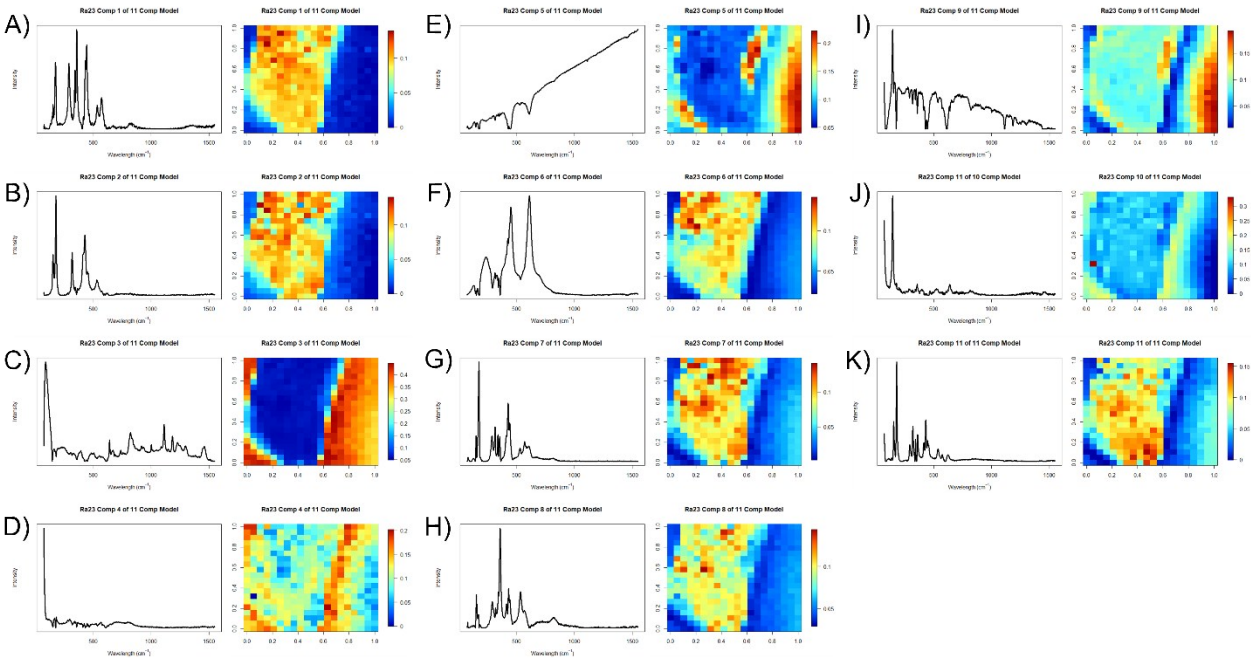

Figure S4: Full MCR-ALS results for hyperspectral Raman imaging data set Ra23. Spatially-resolved chemical images and corresponding resolved Raman spectra generated from an 11 component MCR-ALS model applied to hyperspectral Raman imaging data set Ra23 are shown for each component—component 1 (A), component 2 (B), component 3 (C), component 4 (D), component 5 (E), component 6 (F), component 7 (G), component 8 (H), component 9 (I), component 10 (J), and component 11 (K).

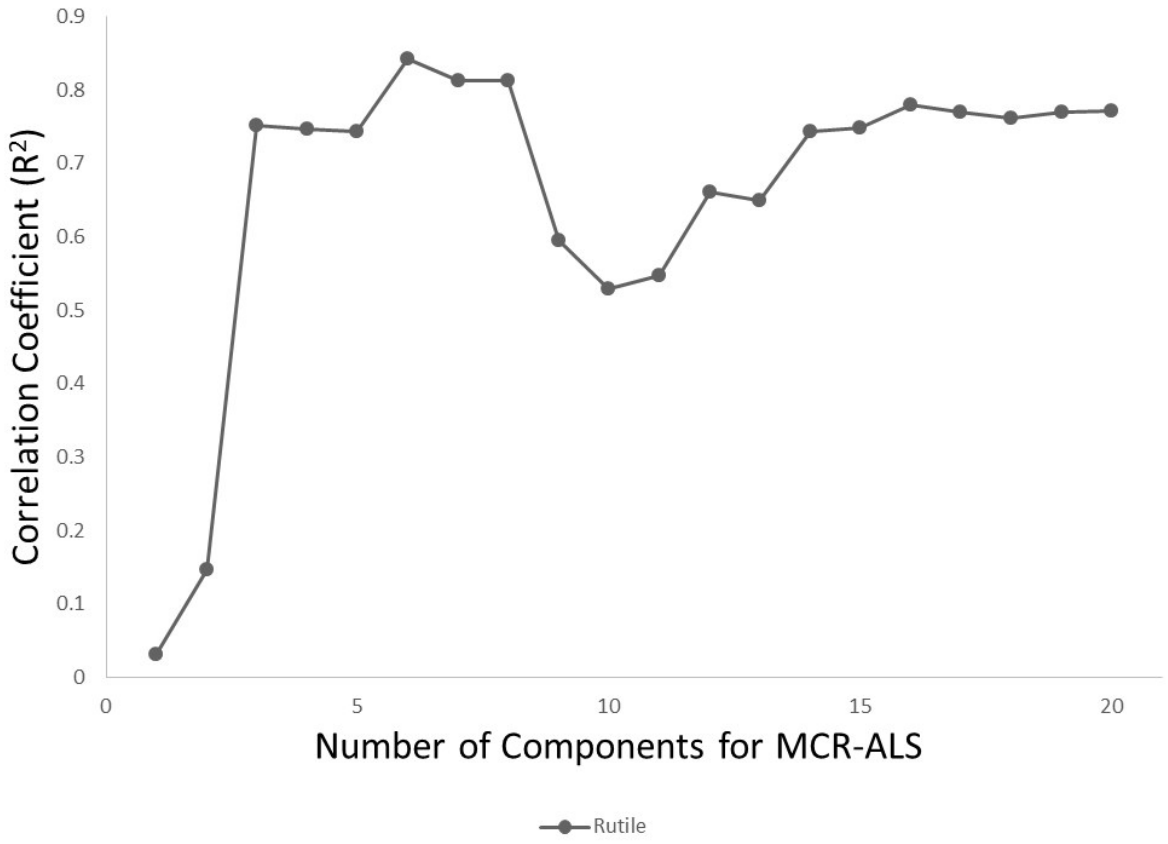

Figure S5: Correlation results for MCR-ALS models applied to hyperspectral Raman imaging data set Ra1. The resolved Raman spectra generated from MCR-ALS were quantitatively compared to target Raman spectra of reference materials, in which correlation coefficients were generated for each individual comparison. The maximum correlation coefficient is plotted for each chemical species within the given MCR-ALS model. The number of chemical components within each MCR-ALS model was varied from one to twenty.

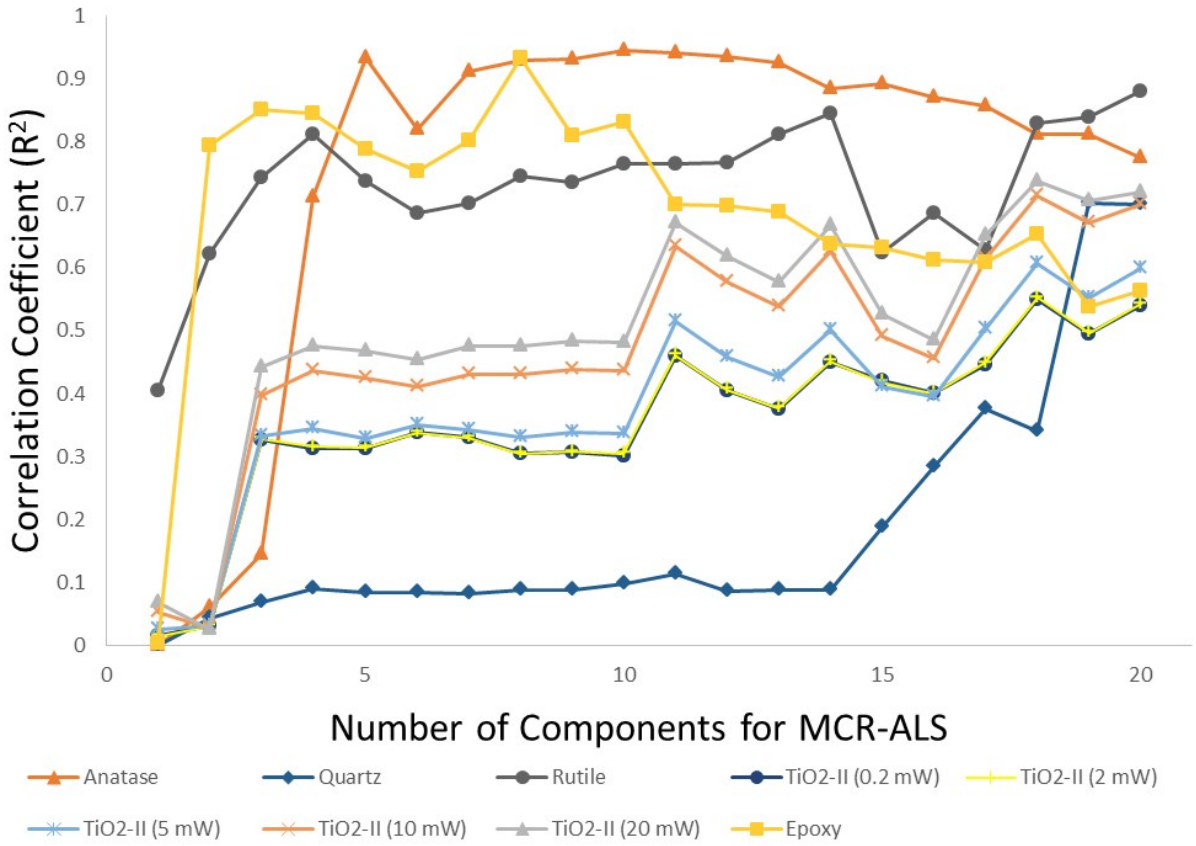

Figure S6: Correlation results for MCR-ALS models applied to hyperspectral Raman imaging data set Ra2. The resolved Raman spectra generated from MCR-ALS were quantitatively compared to target Raman spectra of reference materials, in which correlation coefficients were generated for each individual comparison. The maximum correlation coefficient is plotted for each chemical species within the given MCR-ALS model. The number of chemical components within each MCR-ALS model was varied from one to twenty.

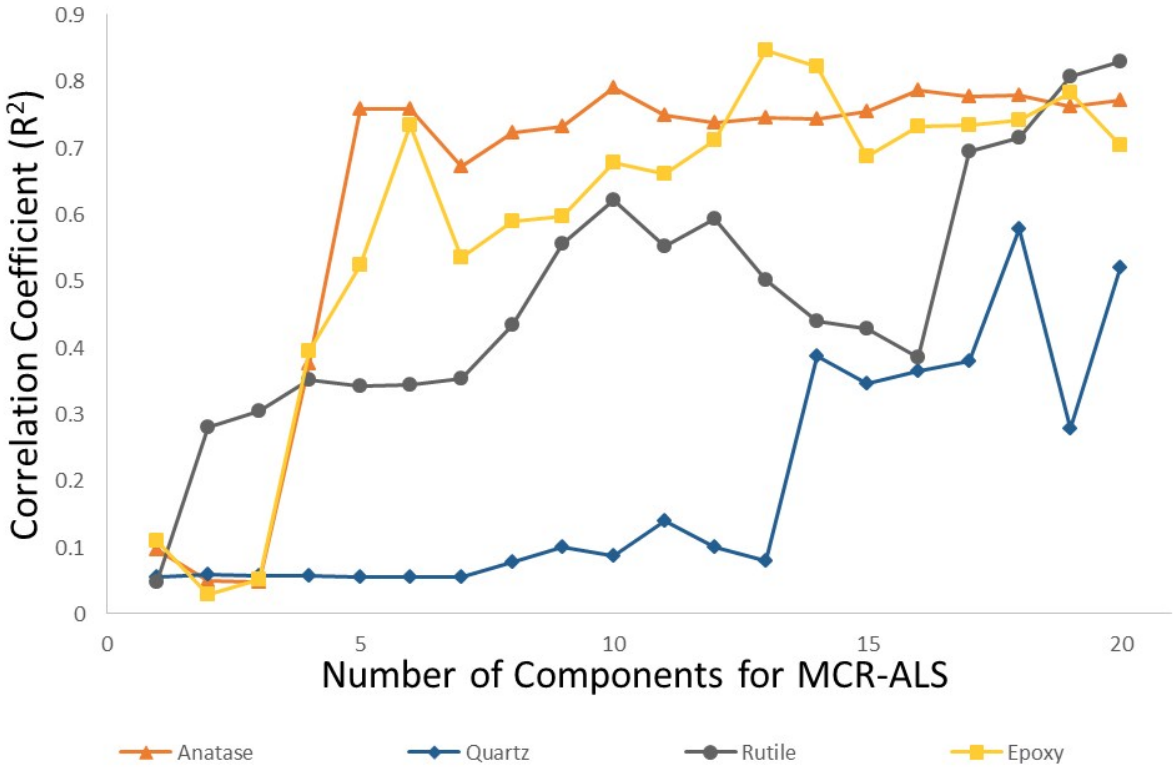

Figure S7: Correlation results for MCR-ALS models applied to hyperspectral Raman imaging data set Ra3. The resolved Raman spectra generated from MCR-ALS were quantitatively compared to target Raman spectra of reference materials, in which correlation coefficients were generated for each individual comparison. The maximum correlation coefficient is plotted for each chemical species within the given MCR-ALS model. The number of chemical components within each MCR-ALS model was varied from one to twenty.

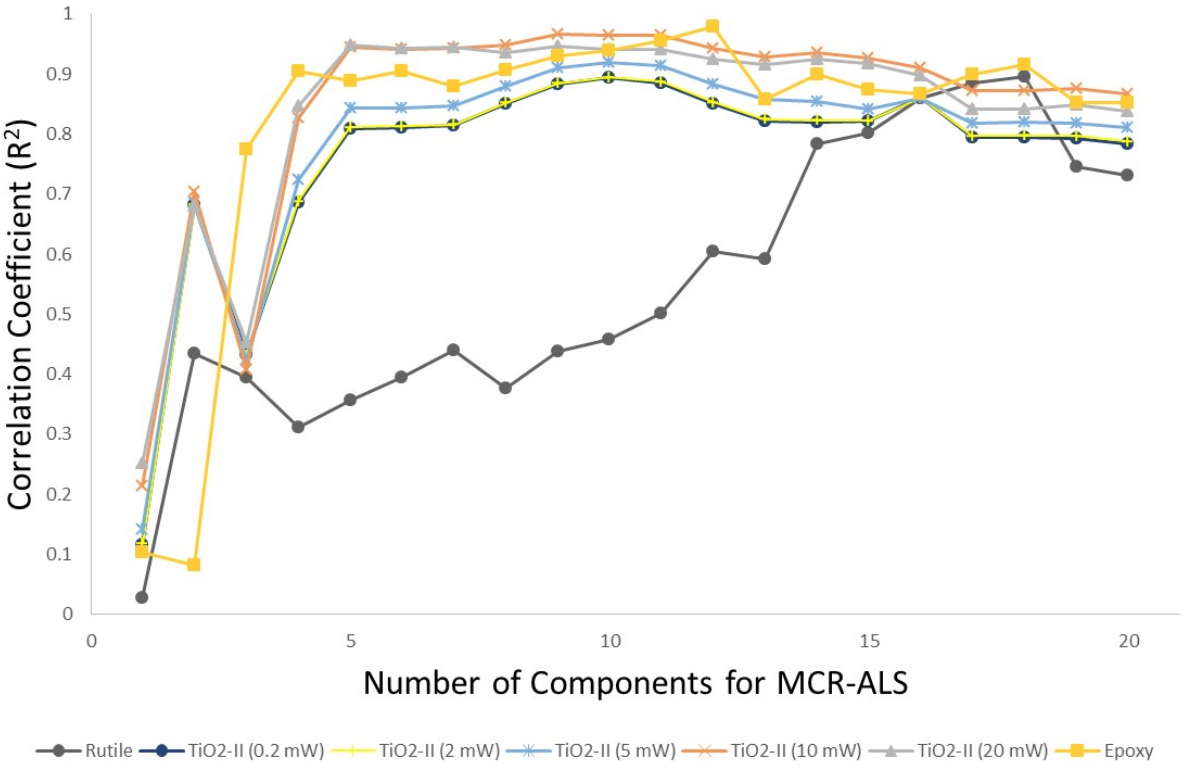

Figure S8: Correlation results for MCR-ALS models applied to hyperspectral Raman imaging data set Ra4. The resolved Raman spectra generated from MCR-ALS were quantitatively compared to target Raman spectra of reference materials, in which correlation coefficients were generated for each individual comparison. The maximum correlation coefficient is plotted for each chemical species within the given MCR-ALS model. The number of chemical components within each MCR-ALS model was varied from one to twenty.

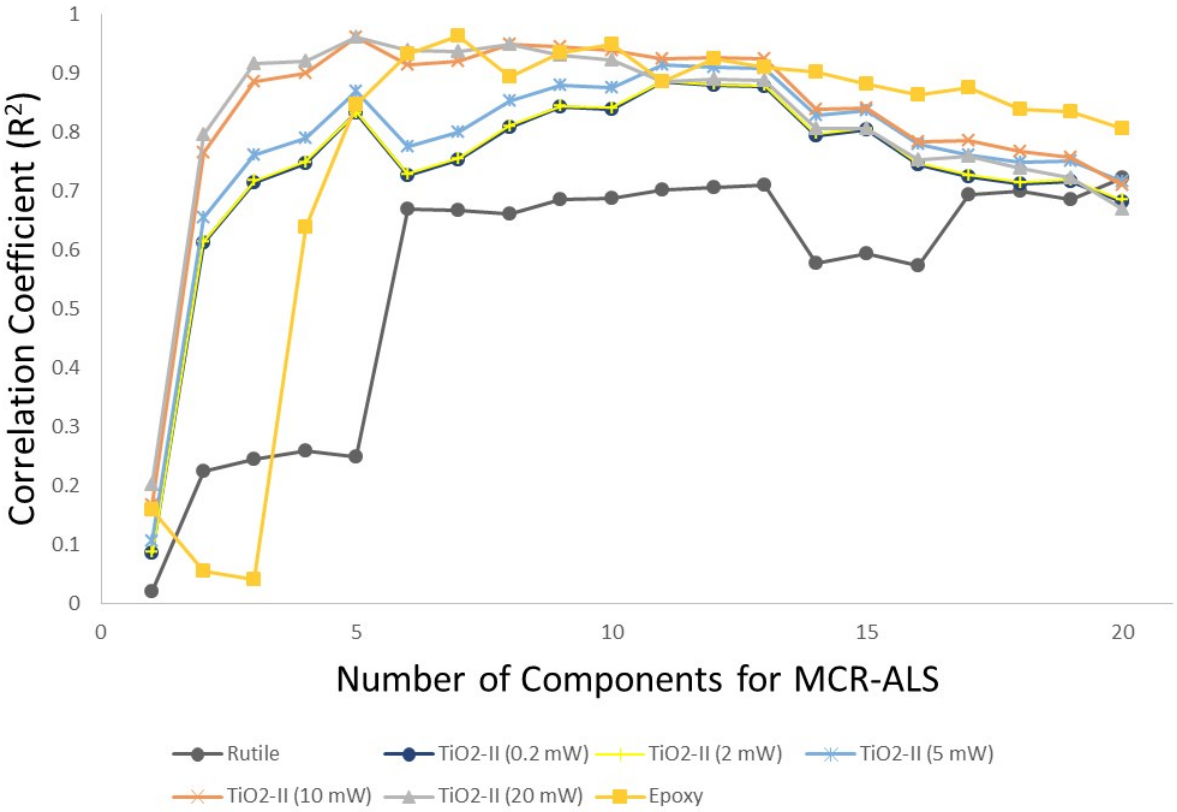

Figure S9: Correlation results for MCR-ALS models applied to hyperspectral Raman imaging data set Ra5. The resolved Raman spectra generated from MCR-ALS were quantitatively compared to target Raman spectra of reference materials, in which correlation coefficients were generated for each individual comparison. The maximum correlation coefficient is plotted for each chemical species within the given MCR-ALS model. The number of chemical components within each MCR-ALS model was varied from one to twenty.

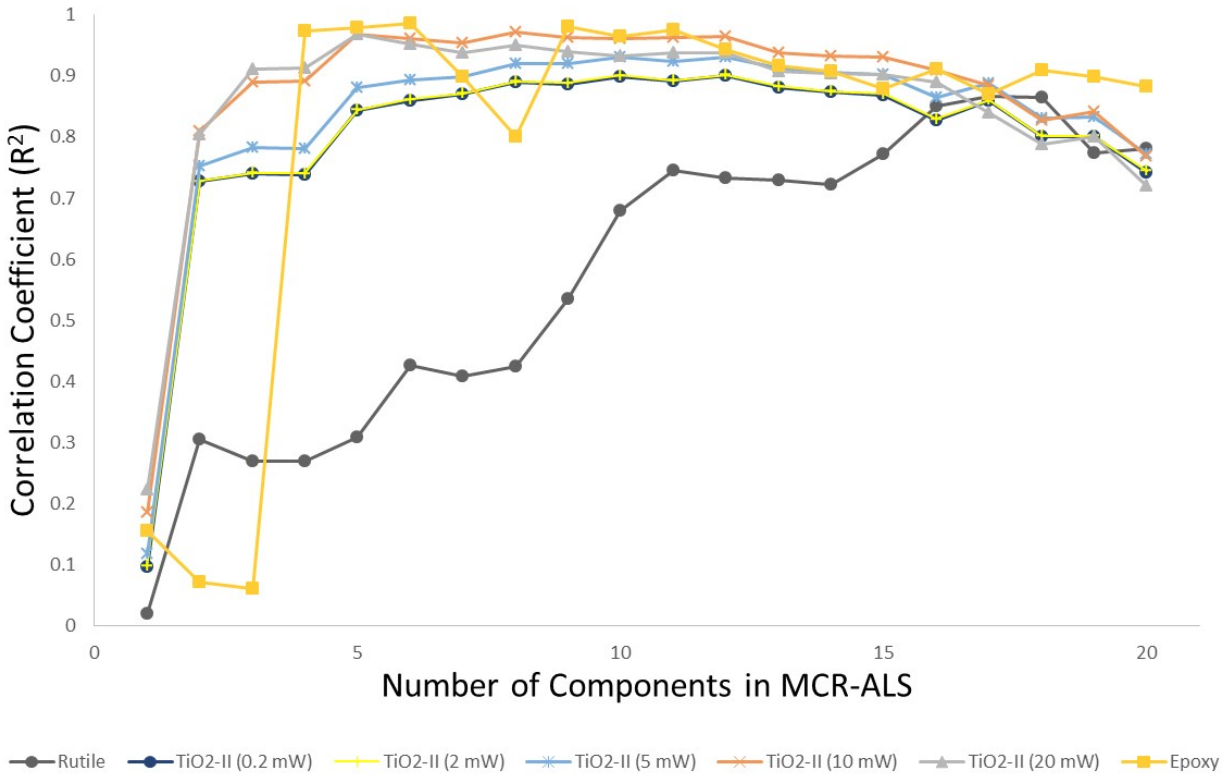

Figure S10: Correlation results for MCR-ALS models applied to hyperspectral Raman imaging data set Ra6. The resolved Raman spectra generated from MCR-ALS were quantitatively compared to target Raman spectra of reference materials, in which correlation coefficients were generated for each individual comparison. The maximum correlation coefficient is plotted for each chemical species within the given MCR-ALS model. The number of chemical components within each MCR-ALS model was varied from one to twenty.

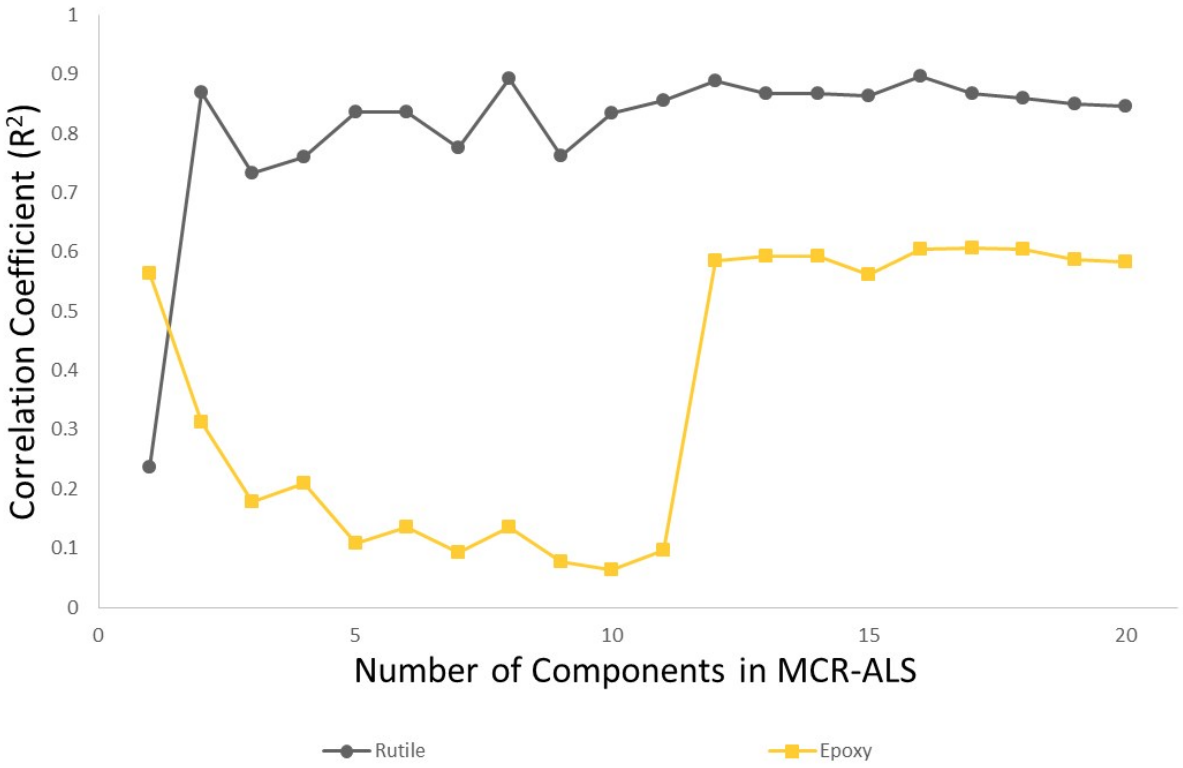

Figure S11: Correlation results for MCR-ALS models applied to hyperspectral Raman imaging data set Ra7. The resolved Raman spectra generated from MCR-ALS were quantitatively compared to target Raman spectra of reference materials, in which correlation coefficients were generated for each individual comparison. The maximum correlation coefficient is plotted for each chemical species within the given MCR-ALS model. The number of chemical components within each MCR-ALS model was varied from one to twenty.

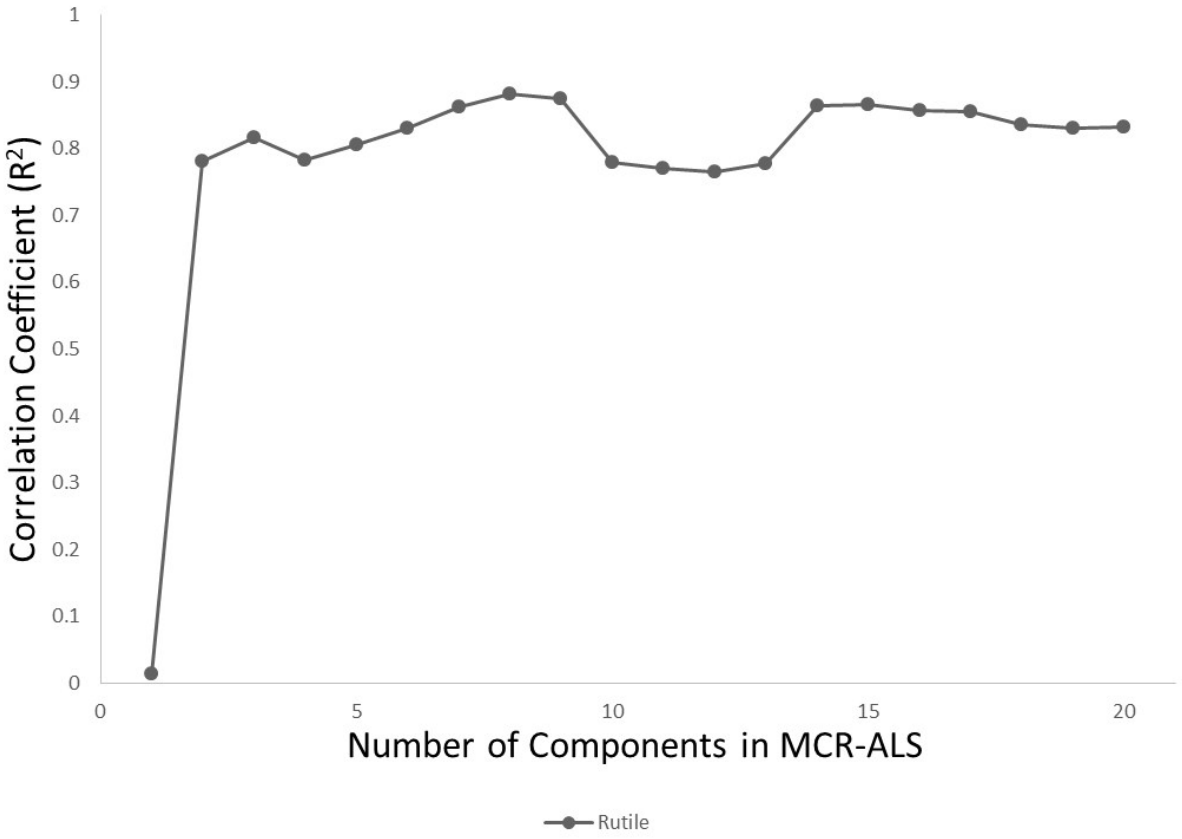

Figure S12: Correlation results for MCR-ALS models applied to hyperspectral Raman imaging data set Ra8. The resolved Raman spectra generated from MCR-ALS were quantitatively compared to target Raman spectra of reference materials, in which correlation coefficients were generated for each individual comparison. The maximum correlation coefficient is plotted for each chemical species within the given MCR-ALS model. The number of chemical components within each MCR-ALS model was varied from one to twenty.

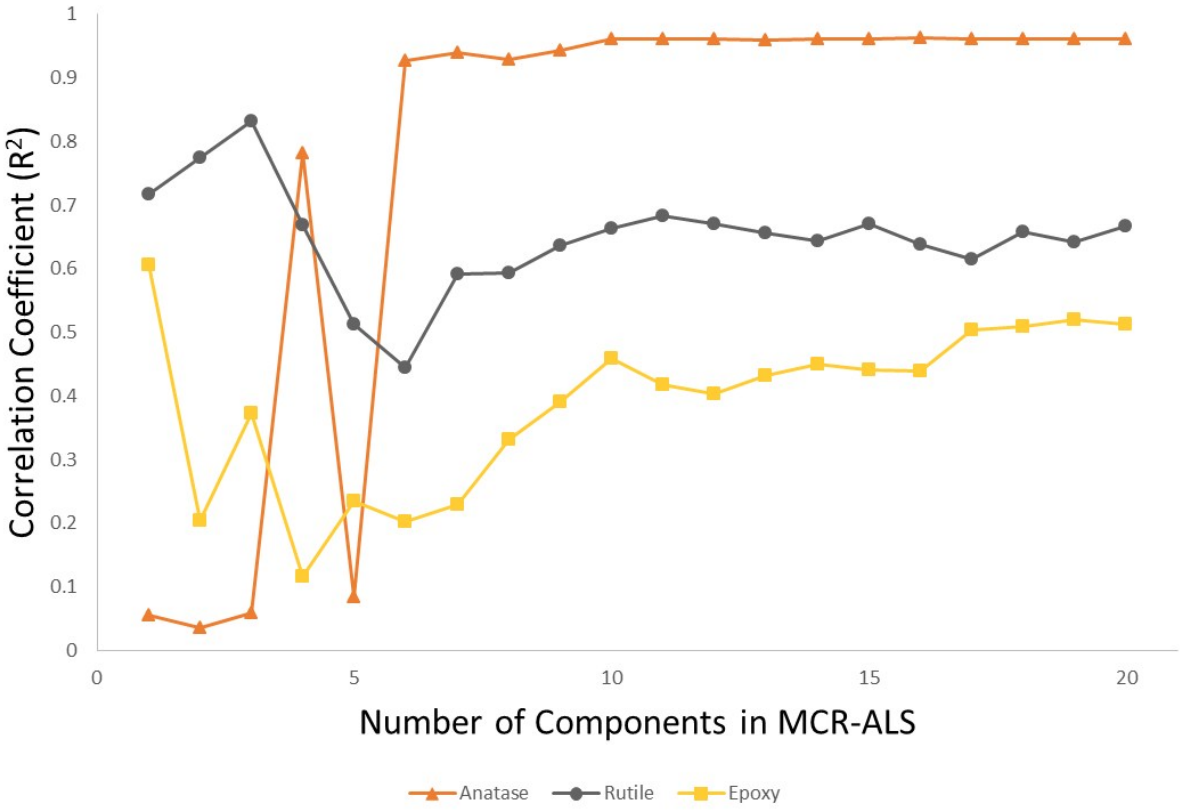

Figure S13: Correlation results for MCR-ALS models applied to hyperspectral Raman imaging data set Ra9. The resolved Raman spectra generated from MCR-ALS were quantitatively compared to target Raman spectra of reference materials, in which correlation coefficients were generated for each individual comparison. The maximum correlation coefficient is plotted for each chemical species within the given MCR-ALS model. The number of chemical components within each MCR-ALS model was varied from one to twenty.

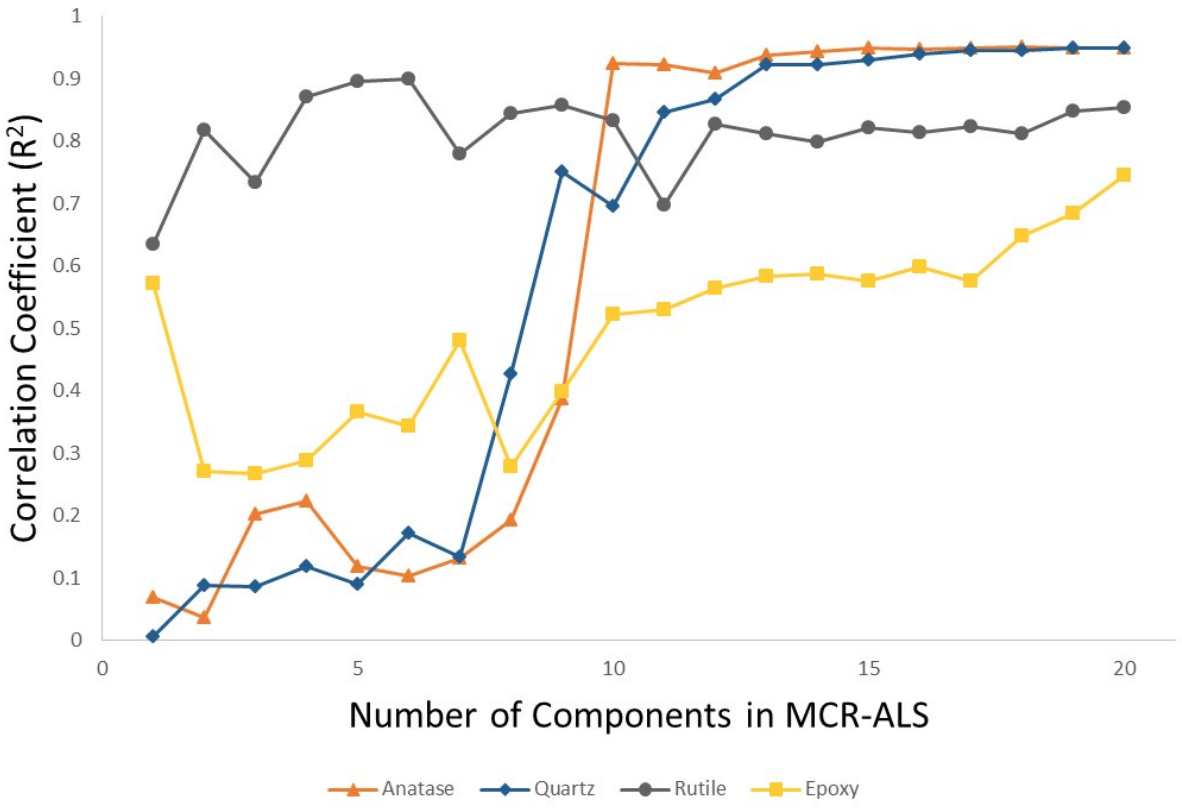

Figure S14: Correlation results for MCR-ALS models applied to hyperspectral Raman imaging data set Ra10. The resolved Raman spectra generated from MCR-ALS were quantitatively compared to target Raman spectra of reference materials, in which correlation coefficients were generated for each individual comparison. The maximum correlation coefficient is plotted for each chemical species within the given MCR-ALS model. The number of chemical components within each MCR-ALS model was varied from one to twenty.

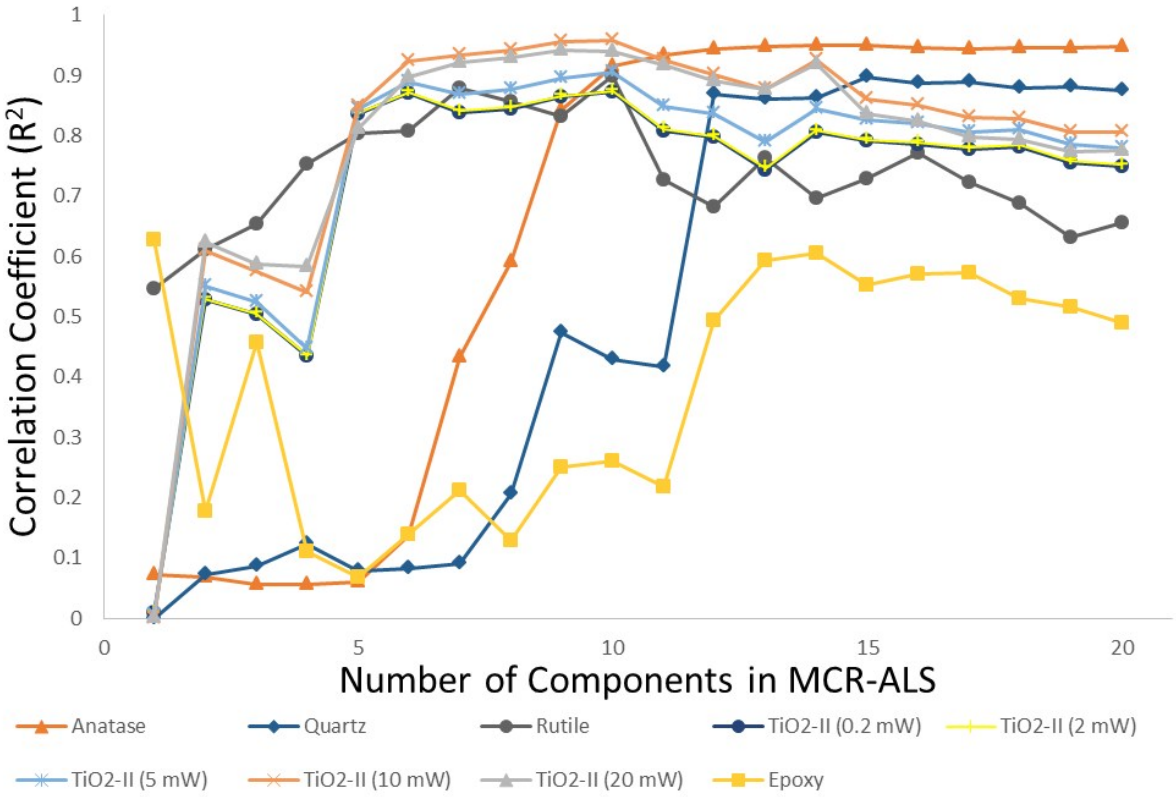

Figure S15: Correlation results for MCR-ALS models applied to hyperspectral Raman imaging data set Ra11. The resolved Raman spectra generated from MCR-ALS were quantitatively compared to target Raman spectra of reference materials, in which correlation coefficients were generated for each individual comparison. The maximum correlation coefficient is plotted for each chemical species within the given MCR-ALS model. The number of chemical components within each MCR-ALS model was varied from one to twenty.

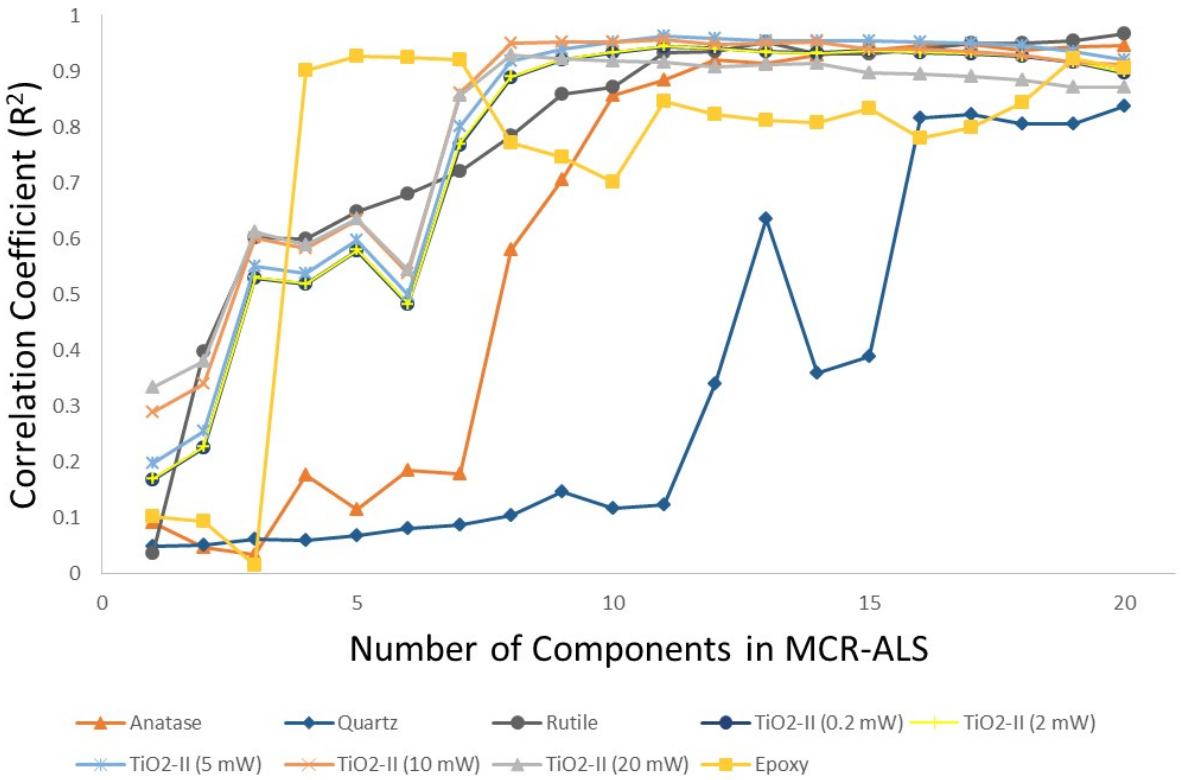

Figure S16: Correlation results for MCR-ALS models applied to hyperspectral Raman imaging data set Ra12. The resolved Raman spectra generated from MCR-ALS were quantitatively compared to target Raman spectra of reference materials, in which correlation coefficients were generated for each individual comparison. The maximum correlation coefficient is plotted for each chemical species within the given MCR-ALS model. The number of chemical components within each MCR-ALS model was varied from one to twenty.

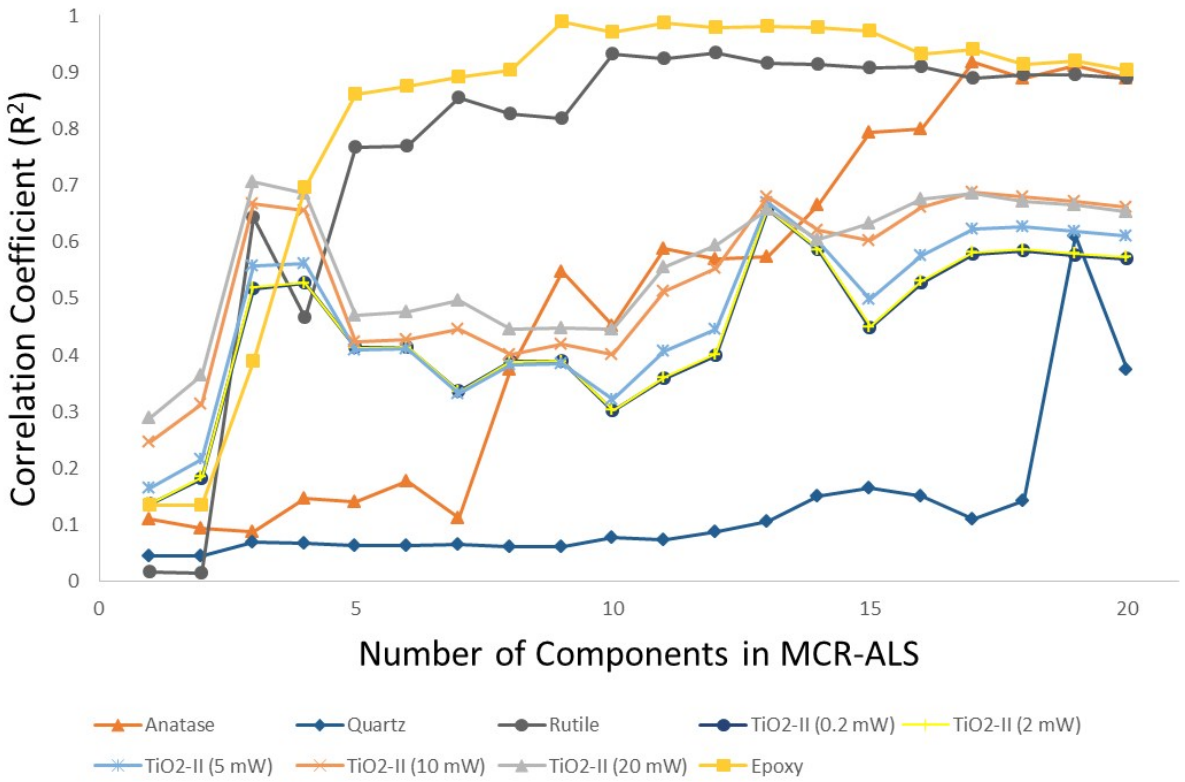

Figure S17: Correlation results for MCR-ALS models applied to hyperspectral Raman imaging data set Ra13. The resolved Raman spectra generated from MCR-ALS were quantitatively compared to target Raman spectra of reference materials, in which correlation coefficients were generated for each individual comparison. The maximum correlation coefficient is plotted for each chemical species within the given MCR-ALS model. The number of chemical components within each MCR-ALS model was varied from one to twenty.

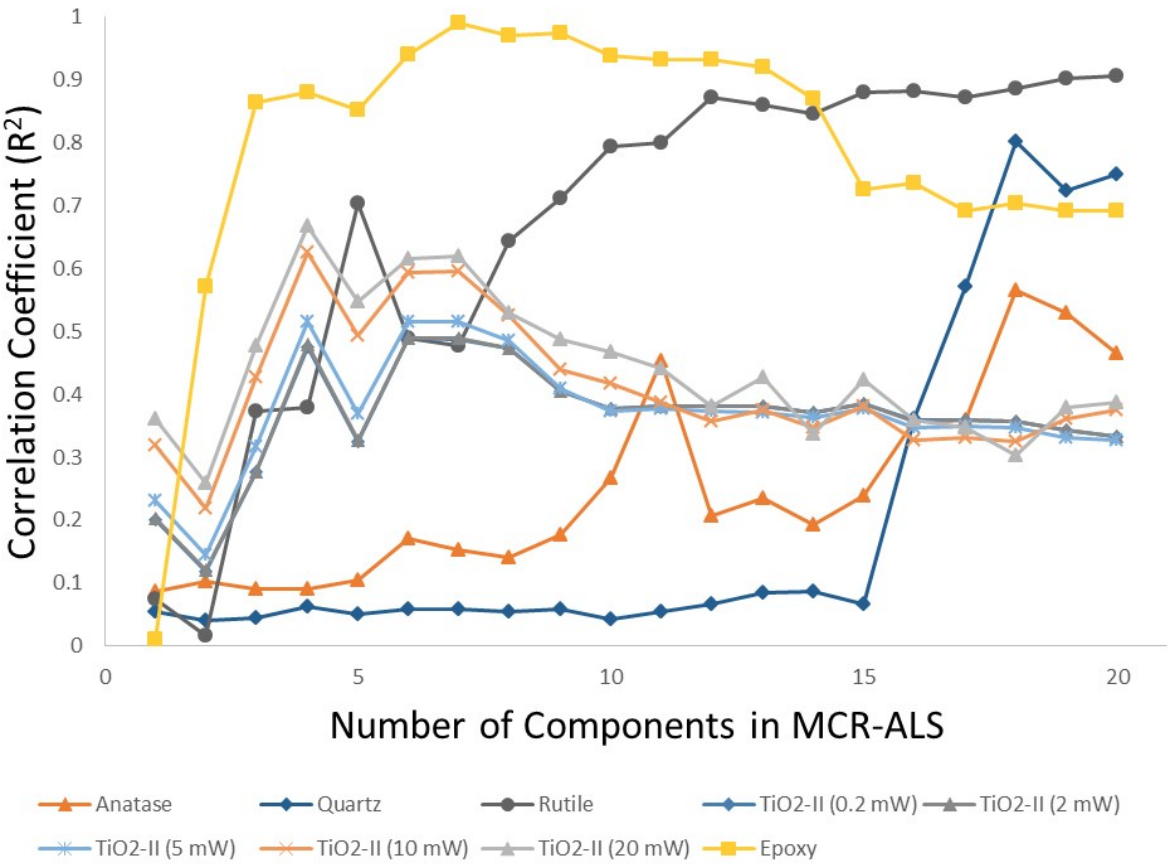

Figure S18: Correlation results for MCR-ALS models applied to hyperspectral Raman imaging data set Ra14. The resolved Raman spectra generated from MCR-ALS were quantitatively compared to target Raman spectra of reference materials, in which correlation coefficients were generated for each individual comparison. The maximum correlation coefficient is plotted for each chemical species within the given MCR-ALS model. The number of chemical components within each MCR-ALS model was varied from one to twenty.

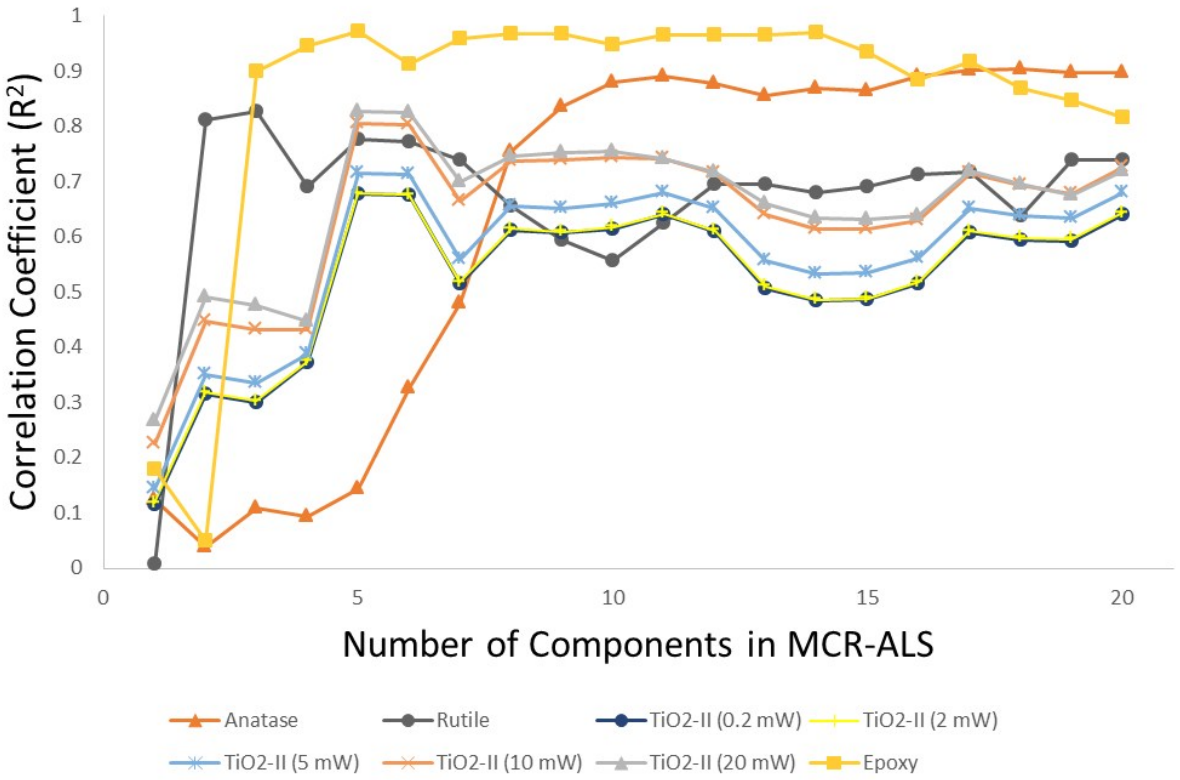

Figure S19: Correlation results for MCR-ALS models applied to hyperspectral Raman imaging data set Ra16. The resolved Raman spectra generated from MCR-ALS were quantitatively compared to target Raman spectra of reference materials, in which correlation coefficients were generated for each individual comparison. The maximum correlation coefficient is plotted for each chemical species within the given MCR-ALS model. The number of chemical components within each MCR-ALS model was varied from one to twenty.

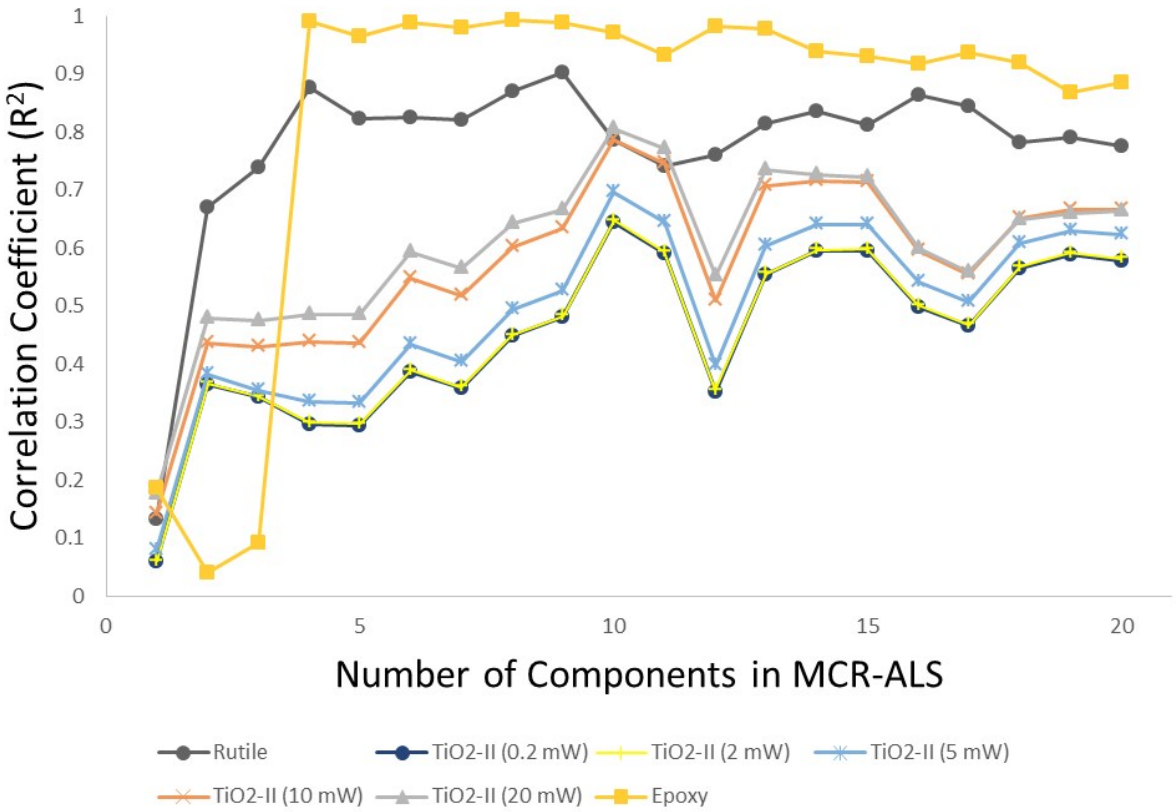

Figure S20: Correlation results for MCR-ALS models applied to hyperspectral Raman imaging data set Ra17. The resolved Raman spectra generated from MCR-ALS were quantitatively compared to target Raman spectra of reference materials, in which correlation coefficients were generated for each individual comparison. The maximum correlation coefficient is plotted for each chemical species within the given MCR-ALS model. The number of chemical components within each MCR-ALS model was varied from one to twenty.

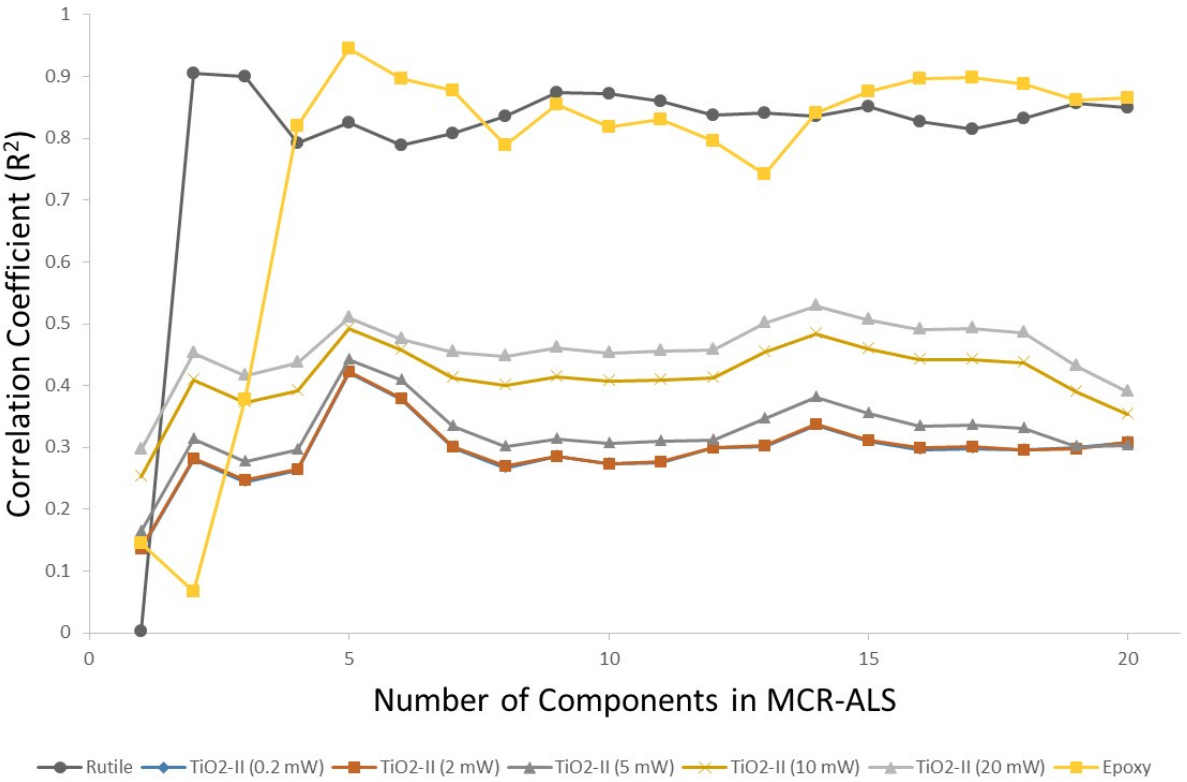

Figure S21: Correlation results for MCR-ALS models applied to hyperspectral Raman imaging data set Ra18. The resolved Raman spectra generated from MCR-ALS were quantitatively compared to target Raman spectra of reference materials, in which correlation coefficients were generated for each individual comparison. The maximum correlation coefficient is plotted for each chemical species within the given MCR-ALS model. The number of chemical components within each MCR-ALS model was varied from one to twenty.

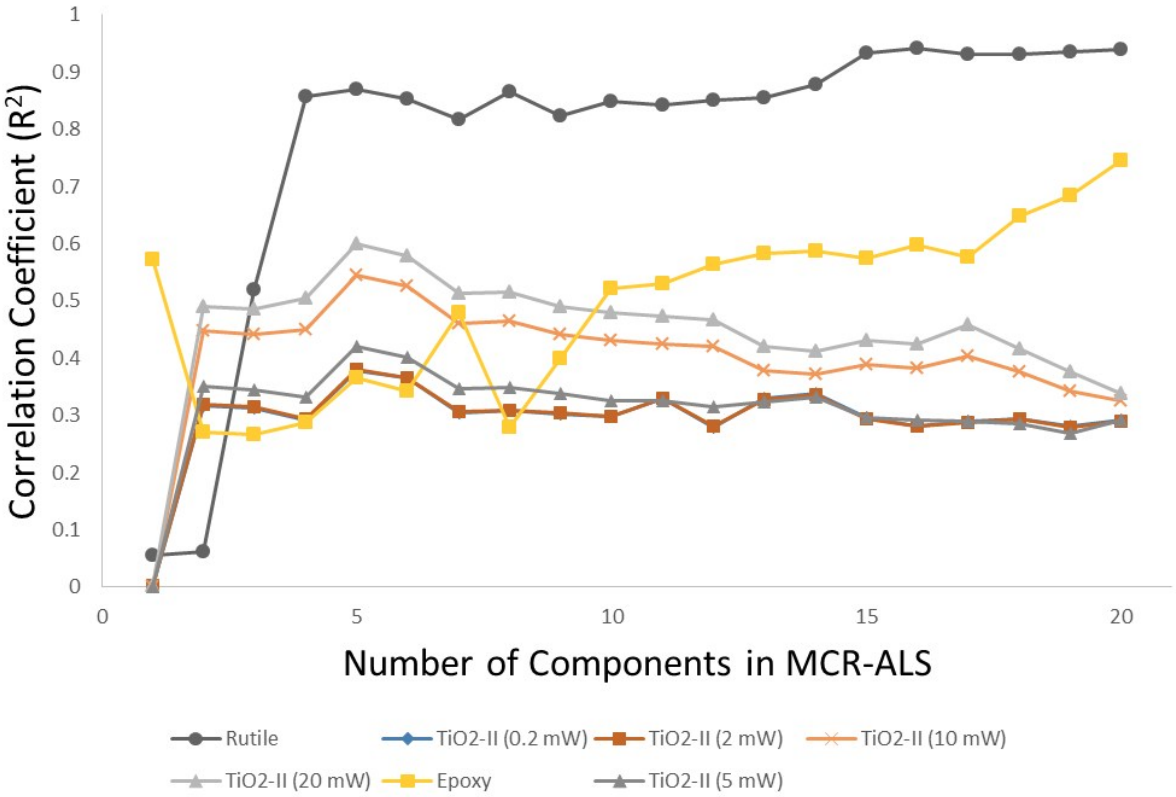

Figure S22: Correlation results for MCR-ALS models applied to hyperspectral Raman imaging data set Ra19. The resolved Raman spectra generated from MCR-ALS were quantitatively compared to target Raman spectra of reference materials, in which correlation coefficients were generated for each individual comparison. The maximum correlation coefficient is plotted for each chemical species within the given MCR-ALS model. The number of chemical components within each MCR-ALS model was varied from one to twenty.

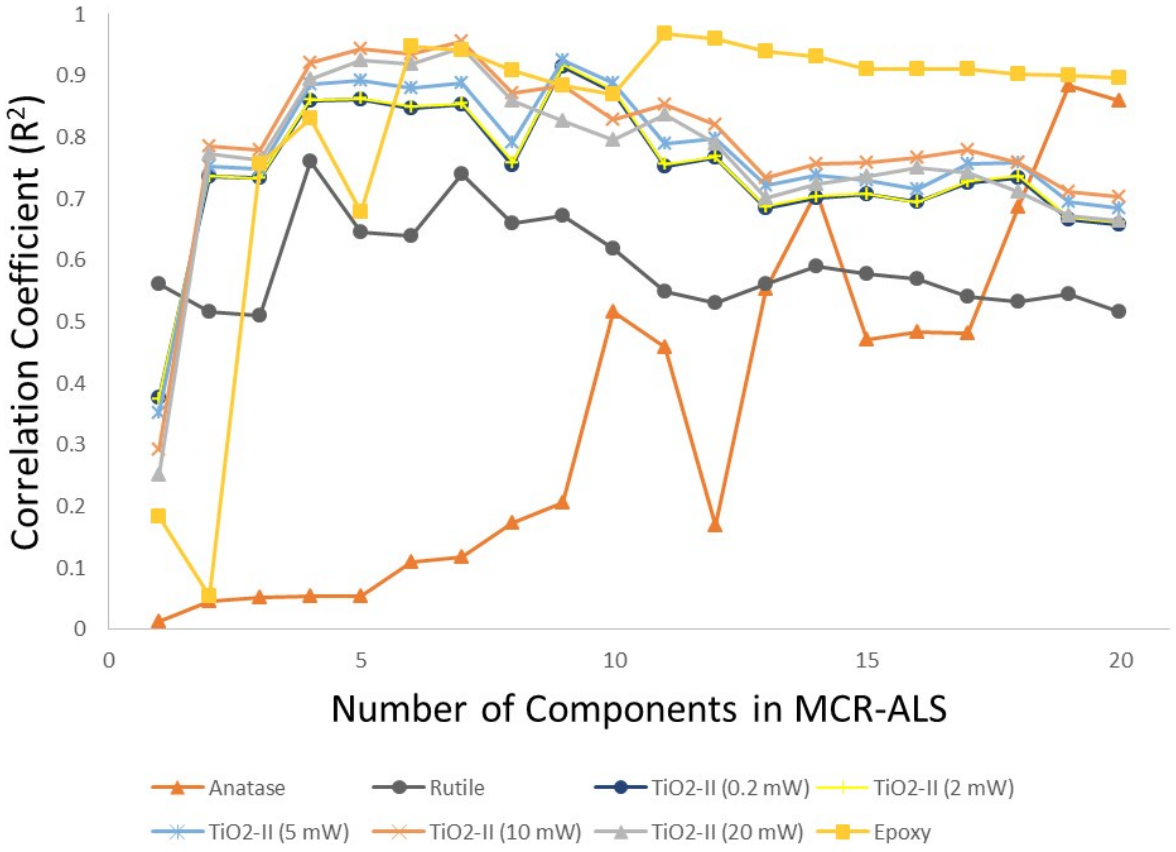

Figure S23: Correlation results for MCR-ALS models applied to hyperspectral Raman imaging data set Ra20. The resolved Raman spectra generated from MCR-ALS were quantitatively compared to target Raman spectra of reference materials, in which correlation coefficients were generated for each individual comparison. The maximum correlation coefficient is plotted for each chemical species within the given MCR-ALS model. The number of chemical components within each MCR-ALS model was varied from one to twenty.

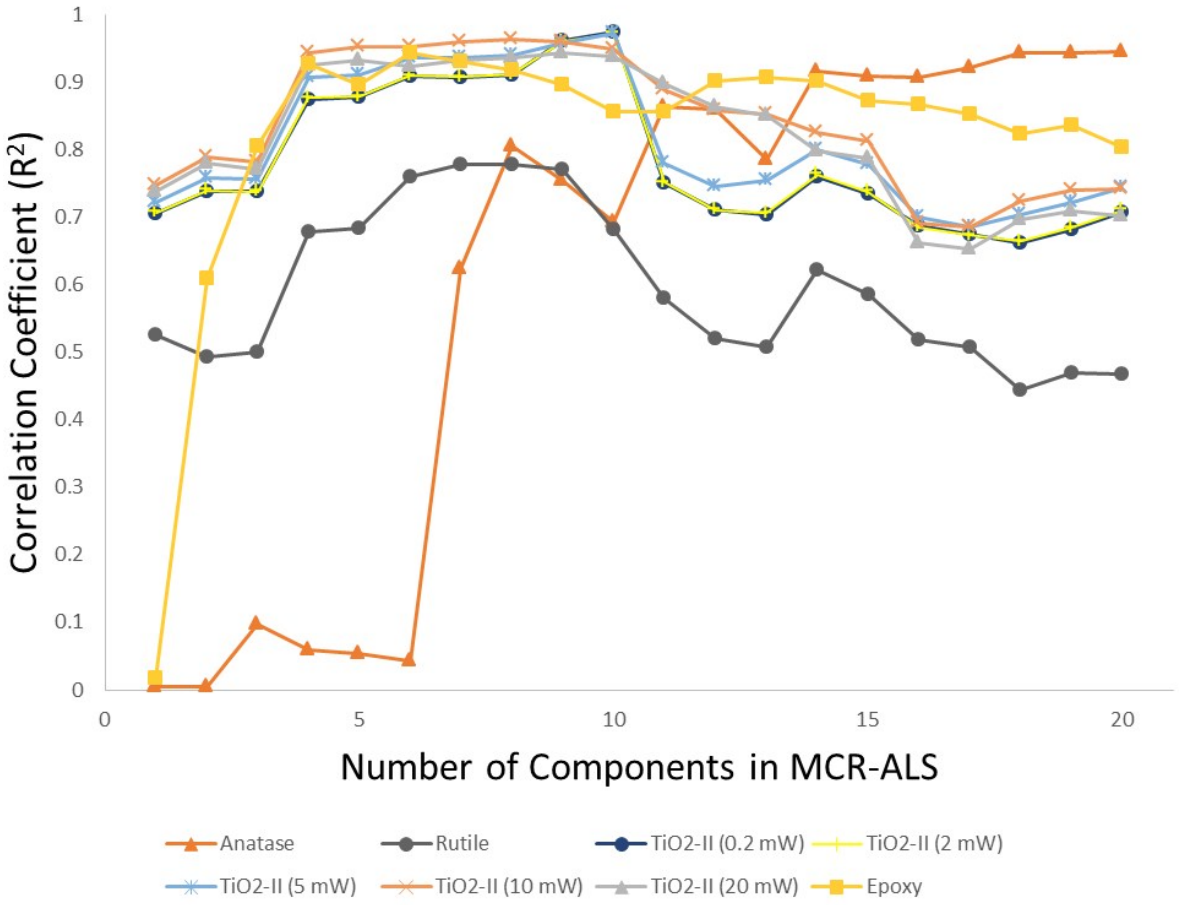

Figure S24: Correlation results for MCR-ALS models applied to hyperspectral Raman imaging data set Ra21. The resolved Raman spectra generated from MCR-ALS were quantitatively compared to target Raman spectra of reference materials, in which correlation coefficients were generated for each individual comparison. The maximum correlation coefficient is plotted for each chemical species within the given MCR-ALS model. The number of chemical components within each MCR-ALS model was varied from one to twenty.

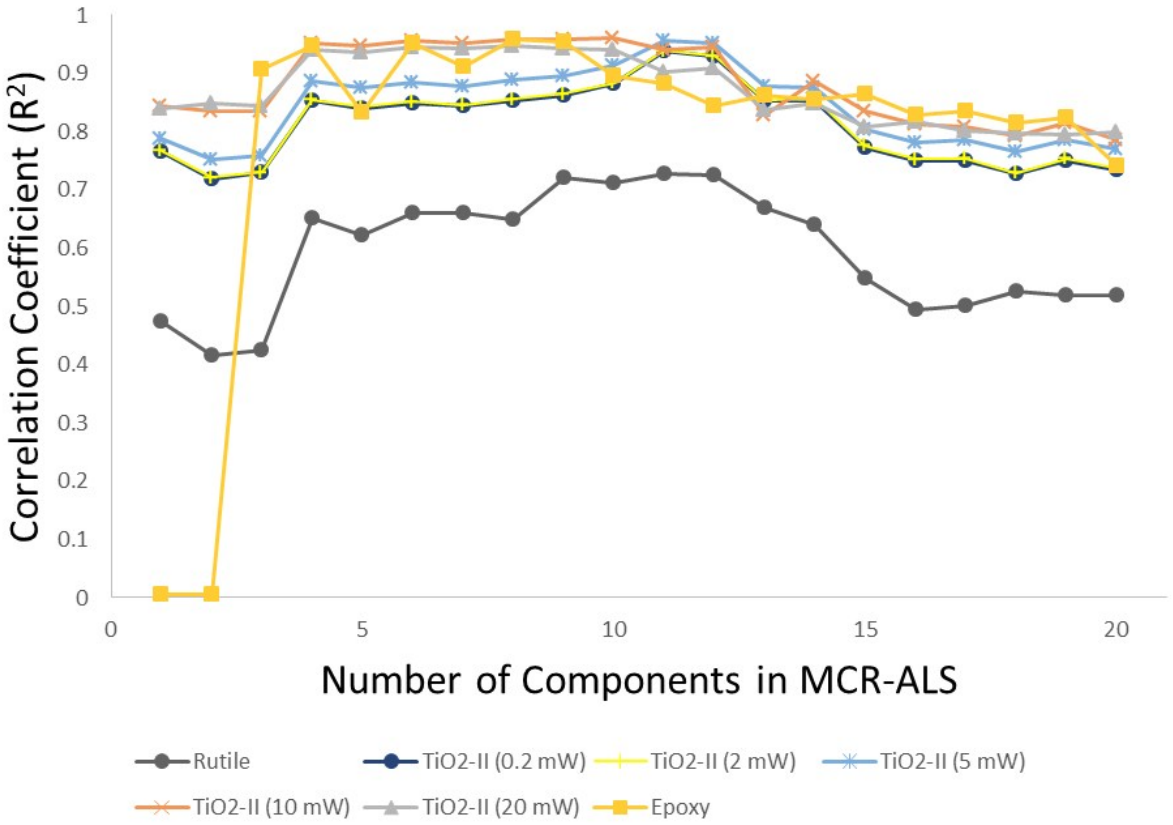

Figure S25: Correlation results for MCR-ALS models applied to hyperspectral Raman imaging data set Ra22. The resolved Raman spectra generated from MCR-ALS were quantitatively compared to target Raman spectra of reference materials, in which correlation coefficients were generated for each individual comparison. The maximum correlation coefficient is plotted for each chemical species within the given MCR-ALS model. The number of chemical components within each MCR-ALS model was varied from one to twenty.

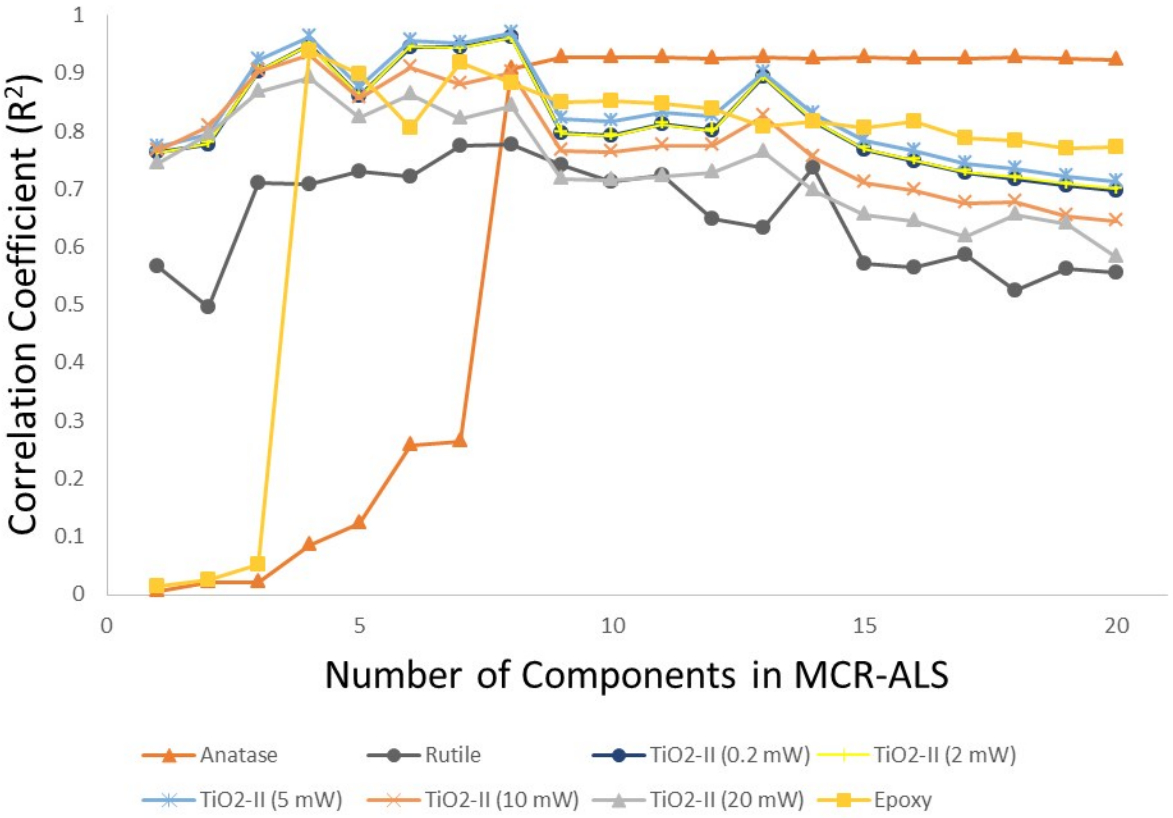

Figure S26: Correlation results for MCR-ALS models applied to hyperspectral Raman imaging data set Ra24. The resolved Raman spectra generated from MCR-ALS were quantitatively compared to target Raman spectra of reference materials, in which correlation coefficients were generated for each individual comparison. The maximum correlation coefficient is plotted for each chemical species within the given MCR-ALS model. The number of chemical components within each MCR-ALS model was varied from one to twenty.

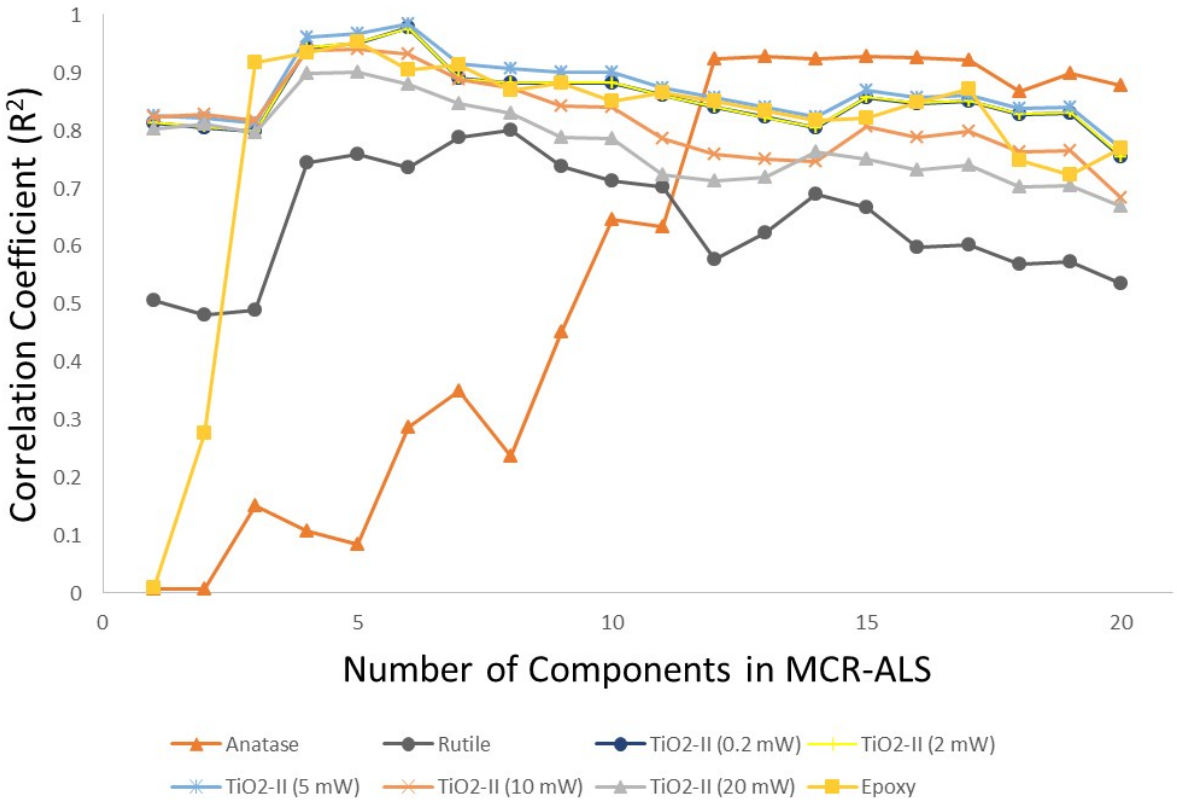

Figure S27: Correlation results for MCR-ALS models applied to hyperspectral Raman imaging data set Ra25. The resolved Raman spectra generated from MCR-ALS were quantitatively compared to target Raman spectra of reference materials, in which correlation coefficients were generated for each individual comparison. The maximum correlation coefficient is plotted for each chemical species within the given MCR-ALS model. The number of chemical components within each MCR-ALS model was varied from one to twenty.

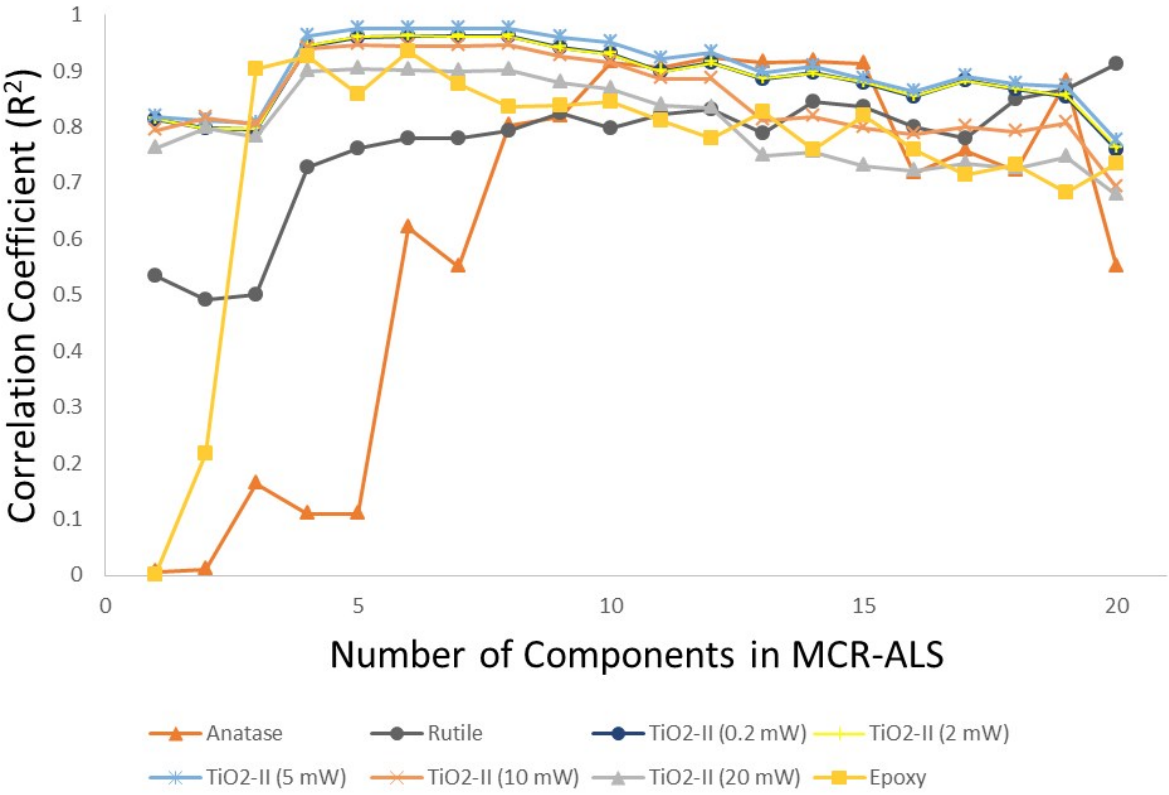

Figure S28: Correlation results for MCR-ALS models applied to hyperspectral Raman imaging data set Ra26. The resolved Raman spectra generated from MCR-ALS were quantitatively compared to target Raman spectra of reference materials, in which correlation coefficients were generated for each individual comparison. The maximum correlation coefficient is plotted for each chemical species within the given MCR-ALS model. The number of chemical components within each MCR-ALS model was varied from one to twenty.

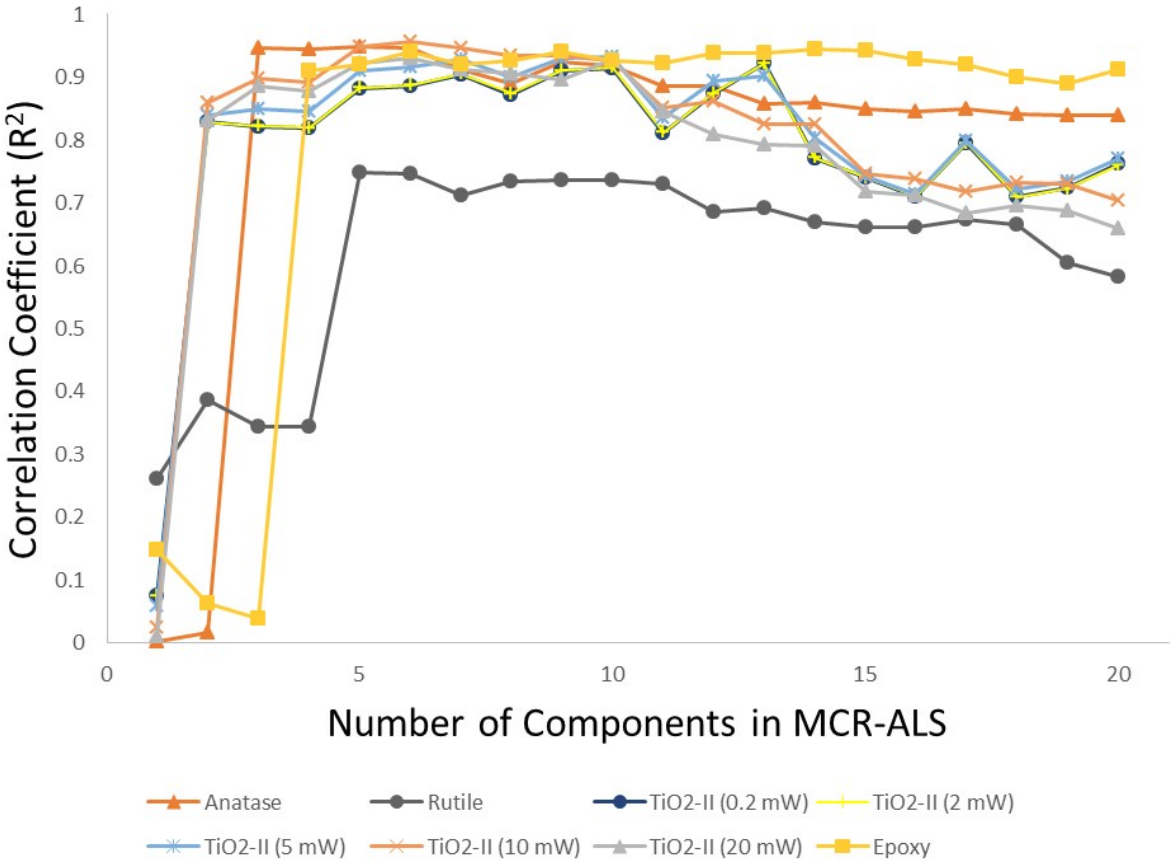

Figure S29: Correlation results for MCR-ALS models applied to hyperspectral Raman imaging data set Ra27. The resolved Raman spectra generated from MCR-ALS were quantitatively compared to target Raman spectra of reference materials, in which correlation coefficients were generated for each individual comparison. The maximum correlation coefficient is plotted for each chemical species within the given MCR-ALS model. The number of chemical components within each MCR-ALS model was varied from one to twenty.

S3. BASELINE EFFECTS OBSERVED IN HYPERSPECTRAL RAMAN IMAGING DATA SET Ra23. Selected Raman spectra within hyperspectral Raman imaging data set Ra23 (**Figure S30)** demonstrate the different baselines observed throughout this experimental data. Non-bilinear spectral baselines are observed, and their variance is larger than that of traditional white noise baselines. As such, additional components in an MCR-ALS model may be needed to resolve these non-bilinear baselines. When investigating trace or minor chemical species, minimal baseline correction is often performed to ensure no chemical information is removed (i.e., excessive spectral correction that removes information concerning the minor chemical species). Using our MCR-ALS methodology, a model can now account for the nonrandom variance in the baseline by using additional components.

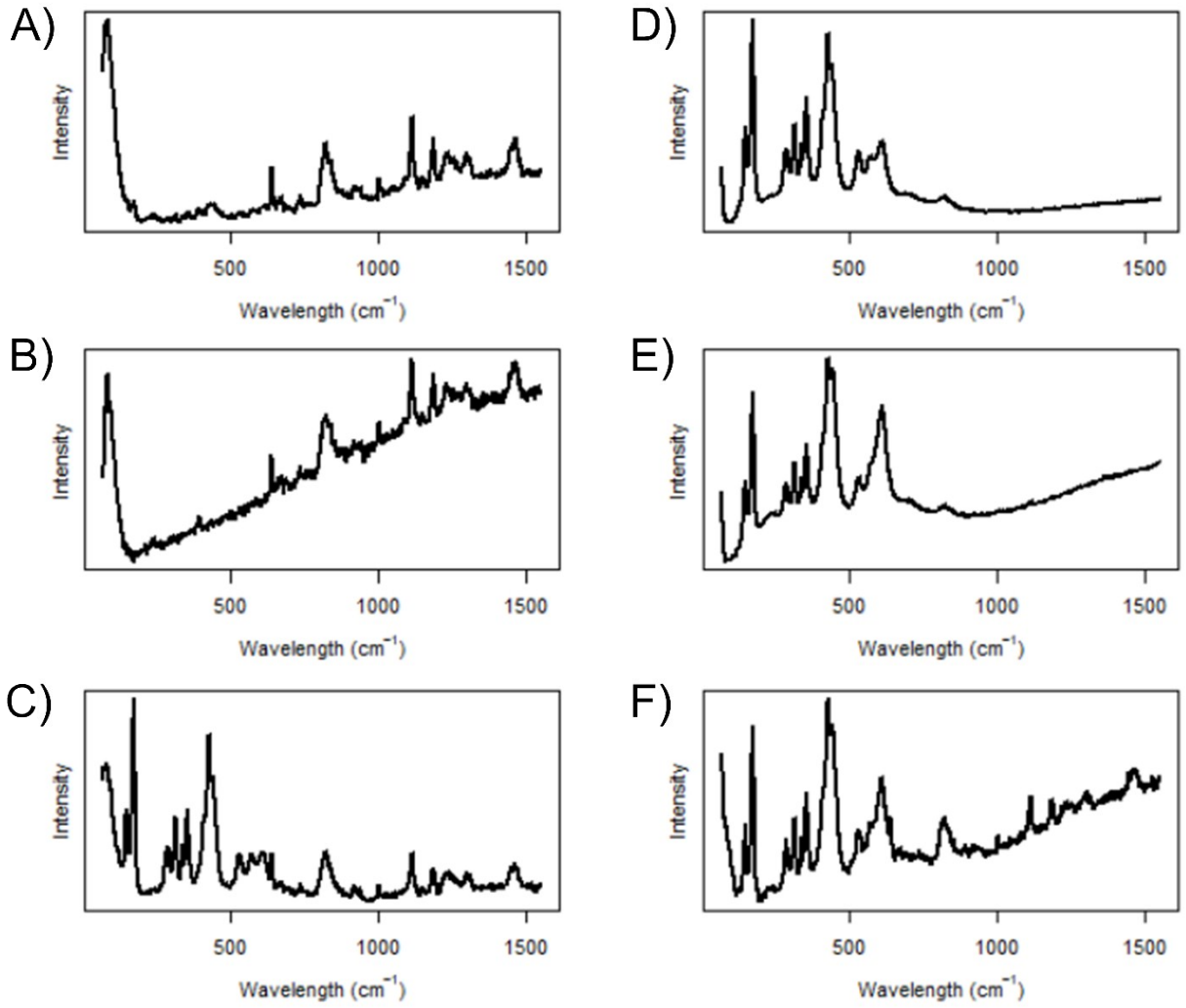

Figure S30: Selected Raman spectra from hyperspectral Raman imaging data set Ra23 are shown. These six Raman spectra (A-F) demonstrate the differences in the spectral baseline observed throughout data set Ra23.

REFERENCES

1. Smith, J. P.; Smith, F. C.; Krull-Davatzes, A. E.; Simonson, B. M.; Glass, B. P.; Booksh, K. S., Raman Microspectroscopic Mapping with Multivariate Curve Resolution-Alternating Least Squares (MCR-ALS) of the High-Pressure, α-PbO_2-Structured Polymorph of Titanium Dioxide, TiO_2-II. *Chemical Data Collections* **2017,** *9-10*, 35-43.